Hydrogels-Based Drug Delivery System with Molecular Imaging

Keun Sang Oh and Soon Hong Yuk

Abstract Drug delivery systems with molecular imaging capability are usually nanoscopic therapeutic systems that incorporate therapeutic agents and diagnostic imaging probes. Polymers (which form hydrogels) and molecular imaging probes used currently were reviewed firstly. Polymer-coated molecular imaging probes were also reviewed to introduce the basic component in the preparation of drug delivery systems with molecular imaging capability. Finally, the recent studies on the drug delivery systems with molecular imaging capability were summarized and their prospect was addressed.

Introduction

Hydrogels, a three dimensional polymer network, may absorb a large quantity of contact liquid. Because of this swelling phenomenon, hydrogels gives a new insight into a model system for the study of a viscoelastic body that is a major topic in polymer physics. In addition to its importance in science, it has many direct applications in the biomedical area, especially in the area of drug and cell delivery.

The concept of drug delivery system in the pharmaceutical area has been investigated using hydrogels as a candidate material. The three dimensional network of hydrogels demonstrated the sustained release of loaded drug [1–3]. Because of presence of a large quantity of water, the swelling transition in response to various stimuli (pH, temperature, light, ionic concentration, metabolites…) is being intensively investigated with respect to the concept of stimulus-sensitive drug delivery [3–7]. In addition, hydrogels have the potential to execute cell delivery, such as pancreatic islet transplantation for diabetes. Transplanted islets are subject to immunologically mediated destruction by both autoimmunity and transplant rejection. Hydrogels can be used as a semipermeable, biocompatible membrane to protect the islets from host immune responses [8–10].

Current interest is focused on the development of nanomedicine platforms in drug delivery and molecular imaging applications. This led to the emergence of nanoscopic therapeutic systems that incorporate therapeutic agents and diagnostic imaging probes (Fig. 1). Studies have shown that this multifunctional nanomedicine improves the therapeutic outcome of drug therapy. To efficiently obtain information on nanomedicine (the drug delivery systems with molecular imaging capability), the nanomedicine should have the reservoir to contain drugs and molecular imaging probes.

K.S. Oh and S.H. Yuk • Department of Advanced Materials, Hannam University, 461-6 Jeonmin Dong, Yusung Gu, Daejeon 305-811, Korea
e-mail: shyuk@hnu.kr

R.M. Ottenbrite et al. (eds.), *Biomedical Applications of Hydrogels Handbook*,
DOI 10.1007/978-1-4419-5919-5_10,

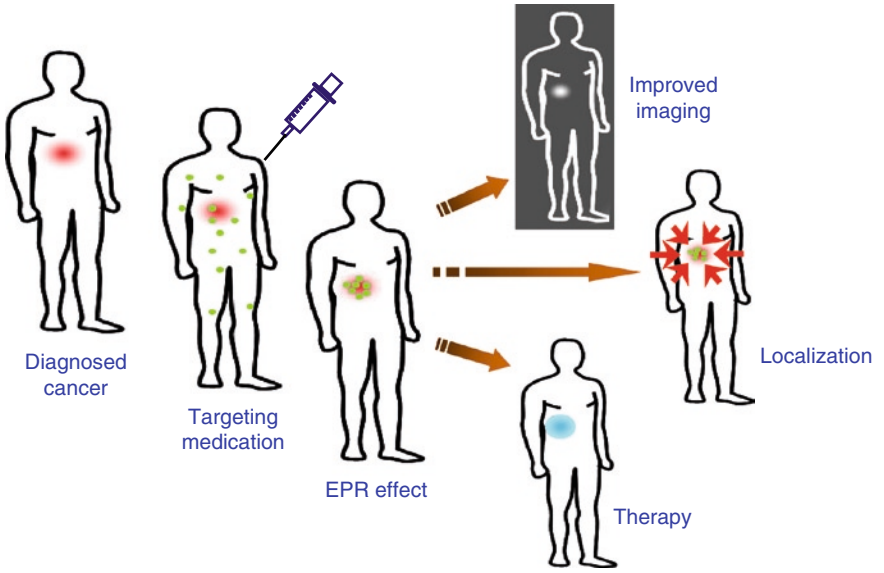

Fig. 1. Therapeutic agents and diagnostic imaging capabilities.

Hydrogels Polymers for Imaging Probes

Poly(vinyl pyrrolidone): Poly(vinyl pyrrolidone) (PVP) is a biocompatible, water-soluble, and nontoxic polymer. Using the hydrogen bonding between the carbonyl groups of PVP and the carboxyl groups of poly(acrylic acid) (PAA) [11] or chitosan [12], various forms of physical gels have been prepared and characterized. PVP gels are utilized as drug delivery systems with the forms of microspheres, nanoparticles, liposomes, and polymer conjugates [13–16].

Self-assembly in aqueous solutions of PVP-block-poly(D,L-lactide) [15], PVP-block-poly(D,L-lactide)-block-PVP, PVP-block-poly(ε-caprolactone)-block-PVP [17], and PVP-block-poly(ε-caprolactone) [18] is a very important property. As a consequence, PVP can be used to form polymeric micelles to deliver the medical drugs or molecular imaging probes.

Poly(vinyl alcohol): Poly(vinyl alcohol) (PVA) is a linear hydrophilic polymer that is nontoxic and biocompatible. Because of intra/intermolecular interactions via hydrogen bonding, PVA forms hydrogels (physical gels). The freeze-thawing method is often used to enhance the mechanical properties [19, 20]. PVA hydrogels are also prepared by chemical crosslinking using irradiation or crosslinkers, such as glutaraldehyde or sodium borate and boric acid [21, 22].

The use of PVA as the base component for hydrogels formation is particularly advantageous, due to the abundance of hydroxyl pendant groups on the PVA chains that can be further substituted with various functional groups. Several research groups have investigated the addition of methacrylate and acrylate pendant groups [23–25], sulfosalicylic acid [26], chitosan [27], hydroxyapatite [28], and alginate [29, 30].

Dextran Hydrogels: Dextran is a polysaccharide consisting of glucose molecules coupled into long branched chains, mainly through 1,6- and some through 1,3-glucosidic linkages. Dextrans are colloidal, hydrophilic, and water-soluble substances that have excellent biocompatibility and hence, they do not affect cell viability. It is susceptible to enzymatic digestion in the body [31]. Dextran has abundant pendant hydroxyl functional groups making it amenable

to chemical modification [32–34]. Hydrophobically modified dextrans are used as stabilizers to produce stable hydrophilic poly(styrene) or poly(lactic acid) nanoparticles by the oil in water (o/w) emulsion and evaporation technique [35–37].

An interconnected macroporous glycidyl methacrylated dextran (Dex-GMA)/gelatin hydrogels scaffold containing microspheres loaded with bone morphogenetic proteins (BMP) has been developed [38]. Microspheres are formed when gelatin was mixed with glycidyl methacrylate dextrans (Dex-GMA); the characteristics of the dextran-co-gelatin hydrogels microspheres can be controlled by the crosslinking density and added substituents to Dex-GMA. Controlled release of bone morphogenetic proteins was observed from 18 to more than 28 days by changing the hydrogels/microsphere ratio.

As a drug delivery system, doxorubicin conjugated dextran nanoparticles have been prepared to improve its therapeutic efficacy in the treatment of solid tumors [39]. In vivo efficacy test of nanoparticles showed faster regression in tumor volume and increased survival time comparing with drug conjugate and free drug.

Chitosan Hydrogels: Chitosan (poly-b(1,4)-D-glucosamine) is a cationic polysaccharide which is obtained by alkaline deacetylation of chitin, the main exoskeletal component in crustaceans. Its molecular weight ranges from 3,000 to 10,000, with a degree of deacetylation from 30 to 95%, depending on the source and preparation method. The amine groups of chitosan are protonated in the acidic conditions (pH < 4). The quality and properties of chitosan products, such as purity, viscosity, deacetylation, and molecular weight, may vary widely because of many factors in the manufacturing process can influence the characteristics of the final product. Chitosan has biodegradability, nontoxicity, biocompatibility, and antifungal activity; chitosan and its derivatives have been studied as biomaterials which are used for drug delivery systems [40] and scaffolds for tissue engineering [41, 42].

Chitosan beads are prepared by simultaneous crosslinking with glutaraldehyde and precipitation in aqueous NaOH [40]. Metronidazole, an antiinfection agent, loaded chitosan beads give faster release at acidic conditions; this pH-sensitive release behavior can be utilized to design targeted delivery system for anticancer drugs.

The differentiation of mesenchymal stem cells (MSCs) and the mass formation of cartilage are possible using an injectable hydrogels composed of copolymer of thermosensitive poly(*N*-isopropylacrylamide) and water-soluble chitosan. Cartilage formation in the submucosal layer of the bladder of rabbits and the in situ hydrogels system composed of dextran copolymer as a scaffold are being pursued [41].

The reactive amino groups in the backbone of chitosan make it possible to chemically conjugate various biological molecules such as different ligands and antibodies, which may improve targeting efficiency of the drug to the site of action [43, 44]. Chitosan-based polymeric vesicles and niosomes bearing glucose or transferrin ligands for drug targeting have been prepared [43]. Transferrin (TF) coupled to the surface of the polymeric vesicles appears to be accessible to the TF receptor in the A431 cell line. The TF receptors are over expressed on the surface of many proliferating cells and the active targeting of polymeric vesicles for drug/gene delivery can be accomplished.

One of the most useful properties of chitosan is ionic chelation. The strong positive charge of chitosan enables it to bind to negatively charged substrates, such as cholesterol, fats, metal ions, and proteins [45–48]. As a nutritional supplement, chitosan has been reported to reduce lipid absorption in the intestine by binding fatty acids and bile acids and by increasing their excretion [45, 46]. Therefore, oral administration of chitosan inhibits the development of atherosclerosis in individuals with hypercholesterolemia by lowering the serum cholesterol levels.

Alginate: Alginate is a naturally derived anionic polysaccharide, obtained mainly from marine algae; it is widely utilized as a food additive and in drug formulations. Alginate consists of two sugar moieties, 1, 4-linked D-mannuronic acid (M) and L-gluronic acid (G), either block or random sequences [49–53]. Alginate forms complexes with divalent ions, such as Ca^{2+}, Ba^{2+}, and so on [52, 53].

Alginate hydrogels have pH-sensitive swelling transitions that are used in the design of drug delivery systems [54, 55]. Drug release from alginate gels is known to be blocked or sustained at low pH by forming a surface gels cover by deswelling, while drug release is accelerated at neutral pH by the swelling increase [56–59]. Alginate can potentially be used for cell delivery, such as microencapsulation of artificial pancreas [60]. The isolated islets of Langerhans suspended in the alginate aqueous solution are effectively encapsulated in the alginate gels when the solution is treated with divalent cations. For further stabilization of islet-encapsulated alginate gels, the polymer complex (an ionic complex) is usually formed at the surface of alginate gels with polycations, such as poly(L-lysine) [61, 62].

Pluronics: Pluronic is a triblock copolymer of poly(ethylene oxide)–poly(propylene oxide)–poly(ethylene oxide) (PEO–PPO–PEO, Poloxamers, Pluronics). Because of its nontoxicity and ability to form a gels, it is widely used in the pharmaceutical area [63–65]. For example, at 20% (w/v), aqueous solutions of poloxamer 407 form hydrogels at body temperature [66].

Poloxamer 188 (PEO_{80}–PPO_{27}–PEO_{80}, molecular weight: 7,680–9,510) is used in intravenous injections and oral formulations and Poloxamer 407 (PEO_{101}–PPO_{56}–PEO_{101}, molecular weight 9,840–14,600) is used in ophthalmic solutions. The sol–gel phase diagrams of poloxamer 188 and poloxamer 407, as a function of concentrations, are shown in Fig. 2.

In addition to the enhancement of the bioavailability of low-solubility drugs in oral solid dosage forms, Pluronics are used as an emulsifier, solubilizer, dispersant, and wetting agent in the preparation of solid dispersions [67, 68]. When these polymers are bound to the surface of nanospheres by the hydrophobic interaction of the PPO chains, the hydrophilic PEO chains stretch into the surrounding medium creating a steric barrier [69, 70]. This barrier

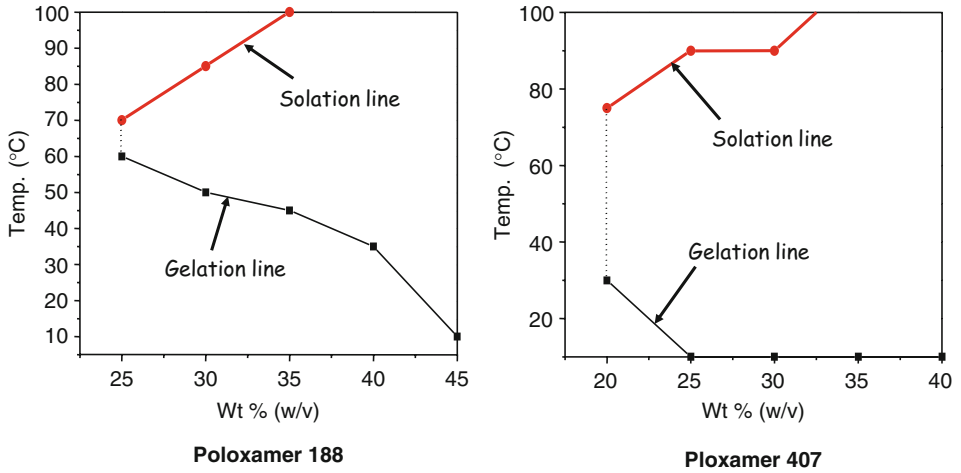

Fig. 2. Sol–gel phase diagram with different concentration of poloxamer 188 and poloxamer 407.

prevents or restricts the adsorption of plasma proteins onto the particle surface decreasing recognition by liver and spleen macrophages [71, 72].

The adsorption of these surfactants is the most widely used procedure to modify the surface characteristics of the primitive carriers; the incorporation of these copolymers into the particles during the manufacturing process has become a significant alternative strategy.

Poly(Ethylene Glycol) (PEG) and Its Copolymers

Poly(ethylene glycol) (PEG) is a neutral, water-soluble, and nontoxic synthetic polymer approved by the FDA for internal use and inclusion in a variety of foods, cosmetics, and drug delivery systems. For prolong blood circulation time, PEG is used to modify nanoparticles to avoid uptake by the reticuloendothelial system (RES). This is important in the design of effective therapeutic systems for injectable delivery and for the controlled drug delivery [73–75].

Modifying the polymer composition, particularly, the middle block composition, the block length, and the block ratio, produced a new generation of PEG–(poly(L-lactic acid-co-glycolide acid))–PEG (PEG–PLGA–PEG) triblock copolymers. The sol–gel transition temperature can be controlled by changing the repeating units of PEG–PLGA–PEG triblock copolymers, such as the PLGA length. As the hydrophobic block (PLGA) length is increased, a stronger shear stress is required to make the gels system. Increasing the PEG length of a PEG–PLGA–PEG triblock copolymer shifts the thermo-phase diagrams to higher temperatures [76, 77].

In situ gels formation in vivo was first made by subcutaneous injection of PEG–PLGA–PEG triblock copolymer aqueous solutions into rats [78]. Based on this phenomenon, paclitaxel-loaded biodegradable polymeric micellar system using low molecular weight and biodegradable amphilic diblock copolymer and monomethoxy PEO_{2000}-Poly(D,L-Lactide)$_{1750}$ micelles (Genexol®-PM) were published by Kim et al. [79, 80]. In Phase I human trials, micellar encapsulation of paclitaxel allowed safer administration of high doses of paclitaxel.

Poly(*N*-isopropylacrylamide) (PNIPAm)

Poly(*N*-isopropylacrylamide) (PNIPAm) is one of the most widely used thermosensitive polymers. PNIPAm has a hydrophilic amide group and a hydrophobic isopropyl group. The linear PNIPAm chain undergoes a rapid dehydration of the hydrophobic isopropyl groups in aqueous solution at its lower critical solution temperature (LCST) of around 32–34°C in water due to its coil-to-globule transition [81–85]. The potential of PNIPAm for drug delivery system [86–89] and cell engineering [90–92] has been well documented. For example, hybrid block and graft copolymers of PNIPAm containing phosphocholine [93, 94], poly(D,L-lactide) [95], and alginate [96, 97] have been successfully synthesized and well characterized as biomaterial candidates.

The copolymers that include the LCST block and a hydrophilic block, such as PEG–PNIPAm copolymers, form micelles above the LCST of PNIPAm, with PNIPAm block forming a micelle core [98]. Block copolymers consisting of the LCST block and a hydrophobic block, such as poly(*N*-isopropylacrylamide)-poly(methyl methacrylate) (PNIPAm–PMMA), form micelles below the LCST, with PMMA block forming a core and PNIPAm block forming a shell [99].

Table 1. Noninvasive imaging in medical application

Technique	Detection	Contrast agent
Computered Tomography (CT)	X-rays	Iodine (Ultravist®), Barium, Barium sulfate Gastrografin
Magnetic Resonance Imaging (MRI)	Magnetic field	Paramagnetic agents: Gd-DTPA(Magnevist®), Gd-DTPA-BMA (Omniscan®)
		Superparamagnetic agents: iron oxide nanoparticles (Resovist®, Feridex®)
Positron Emission Tomography (PET)	Gamma rays	F18-FDG(2-Deoxy-2-fluoro-D-glucose)
Ultra-sonography	Ultrasonic waves	Microbubbles(Albunex®, Levovist®)

Molecular Probes for Imaging

With the advances in imaging technology, the importance of molecular imaging probes has increased for precise diagnosis. The visualization of the cellular function and the follow-up of the molecular process in living organisms without surgical operation are facilely carried out. Some of the techniques used for noninvasive imaging in diagnosis medicine are listed in Table 1.

Gold Nanoparticles

One of the most interesting aspects of gold nanoparticles is that their optical properties are varyingly dependant on the particle size and shape. Bulk gold looks yellow in reflected light, but this characteristic changes to orange, through several tones of purple and red, as particle size is reduced to ~20 nm. These effects are the result of changes in the so-called surface plasmon resonance (SPR) [100].

Gold nanoparticles are usually prepared by reduction in a boiling sodium citrate solution [101]. The formation of gold nanoparticles appears as a deep wine red color and the UV absorption in the aqueous media at around 520 nm. Functionalization of gold nanoparticles (gold surfaces) with molecules containing thiol (-SH), which has a high affinity for gold atoms is commonly used. A number of biosensors are designed based on this phenomenon.

The gold nanoparticles are biocompatible and nontoxic in vivo [102, 103]. However, plasma proteins and salts in the blood nonspecifically adsorb onto the surface of gold nanoparticles, this often causes aggregation; therefore, the direct use of gold nanoparticles in vivo can lead to clearance from the bloodstream due to uptake by the reticular endothelial system (RES) (Kupffer cells of the liver) [104–107]. Therefore, gold nanoparticles used in vivo are usually surface modified with PEG [104].

Magnetic Nanoparticles

Magnetic nanoparticles are manipulated under the influence of a magnetic field and are commonly composed of magnetic elements such as iron oxide (superparamagnetic iron oxide (SPIO) and ultrasuperparamagnetic iron oxide (USPIO)) and gadolinium compounds. Because of difficulties in recognizing tumors from normal tissues by magnetic resonance

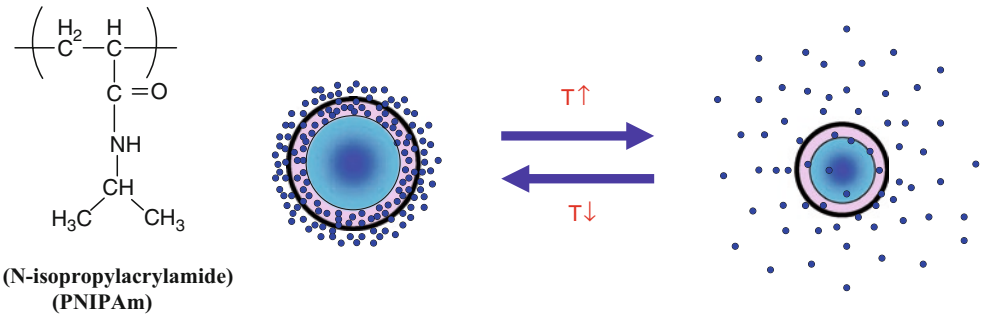

Fig. 3. Schematic description for molecular structure of poly(*N*-isopropylacrylamide) (PNIPAm) and drug release mechanism in response to temperature (T) changes.

imaging (MRI), patients are often injected with a contrast agent, such as iron oxide nanoparticles or gadolinium chelates.

Nanoparticles are prepared by either coprecipitation [108–110], high-temperature decomposition [111–113], or microemulsion [114, 115]. Coprecipitation is a facile and convenient way to synthesize iron oxides (Fe_3O_4 or γ-Fe_2O_3) from aqueous Fe^{2+} and Fe^{3+} salt solutions by the addition of base at room temperature or at raised temperatures. The stability is maintained by electrostatic and repulsive interaction between counter-ions. The size, shape, and composition of the magnetic nanoparticles mainly depend on the type of salts used, the Fe^{2+}/Fe^{3+} molar ratio, reaction temperature, the pH, and ionic strength of the media [116–118].

The high-temperature decomposition (>200°C) of an organic iron precursor in the presence of hydrophobic ligands, such as oleic acid, is typically used; the hydrophobic ligands form a dense coating around the nanoparticles, thereby avoiding their aggregation.

Microemulsions are used to obtain relatively small particles (high surface area) with well controlled properties; water-in-oil microemulsions are usually used to produce iron oxide nanoparticles. The type and concentration of surfactant [119, 120], type of oil [121] and alcohol [122–124], droplet core size [125], and the speed of microemulsion mixing [126] all play an important role in the formation of iron oxide nanoparticles by microemulsion techniques.

Iron oxide nanoparticles have been approved for clinical use, especially for MRI, for example, Endorem® (diameter 80–150 nm, Advanced Magnetics) and Resovist® (diameter 60 nm, Schering) for liver/spleen imaging [127–129].

Gadolinium is also an FDA approved contrast agent for MRI. Gadolinium, or gadodiamide, provides greater contrast between normal tissue and abnormal tissue in the brain and body. Because of their paramagnetic properties, solutions of organic gadolinium complexes and gadolinium compounds are used as intravenous radiocontrast agents to enhance images in medical MRI. After it is injected into a vein, gadolinium accumulates in the abnormal tissue with bright (enhanced) images on the MRI. With the administration of MRI contrast agents, the relaxation times T1 and/or T2 of a proton in the vicinity of an agent change, thus generating image contrast (bright/dark) (Fig. 4) [130].

Fluorescence Dyes

Optical fluorescence depends on the inherent property of fluorophores, such as fluorescein isothiocyanate (FITC) and FITC derivatives, cysteine, cyanine dye (cydye), and Indicynine green dye (ICG) are used for fluorescence imaging (Fig. 5) [130].

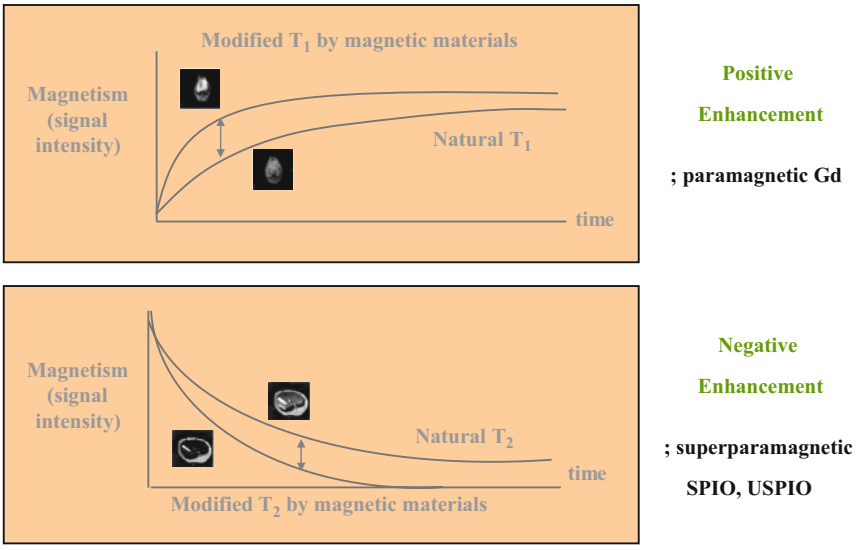

Fig. 4. T1 and T2 relaxation processes [130].

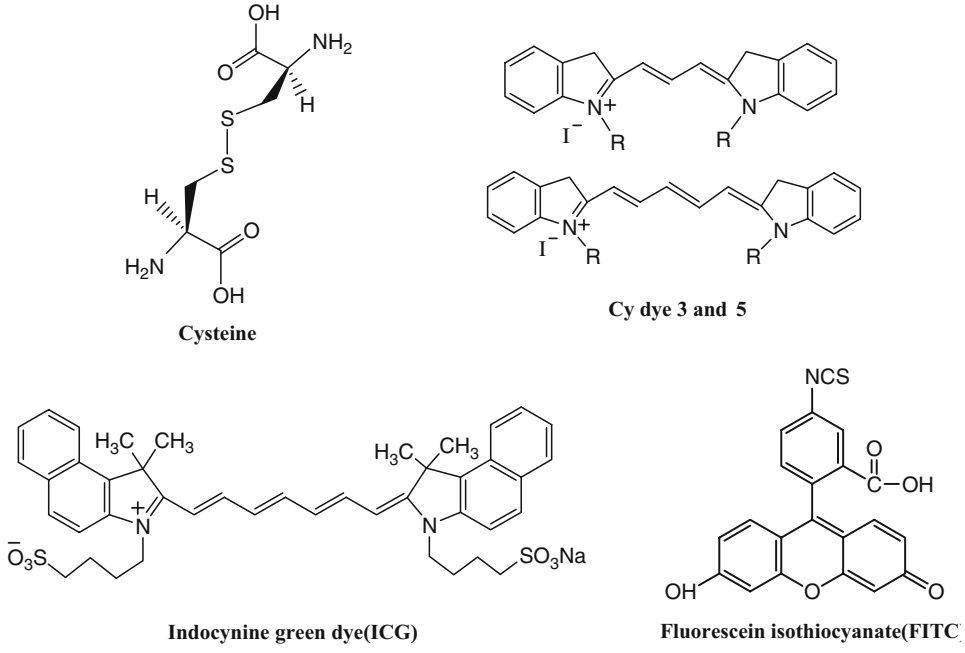

Fig. 5. Various used fluorophores in biological imaging.

Fluorescein isothiocyanate (FITC) is used in several biological applications, such as fluorescent-labeled antibodies and molecules that are taken up by cells or organelles. Usually, the energy from an external source is absorbed by the fluorophores injected or accumulated at the tumor site.

Microbubbles

Ultrasound contrast agents, which consist of a hydrophobic gas (microbubbles) and a stabilizing shell, have enabled clinical contrast echocardiography due to their enhanced stability in circulation. Moderate intensity ultrasound assisted by encapsulated microbubbles has been used in in vitro and in vivo targeting drug delivery via a process called "sonoporation." Ultrasound imaging is used to molecularly target microbubbles to the liver [131], breast [132], and prostate tumors [133].

These advances have created interest in ultrasound as a molecular imaging modality. Ultrasonic imaging of molecular targets associated with angiogenesis [134–137], thrombosis [138], and inflammation is being used [139, 140].

There are two types of bubbles that are related to sonoporation process: free bubbles and encapsulated microbubbles. Free bubbles are usually cavities filled with air, other gases, or gas vapor from surrounding liquid. However, due to their instability, free bubbles are usually encapsulated in biocompatible polymers as microbubbles for the ultrasonic imaging of angiogenesis [136, 141–146].

Quantum Dots

In general, the quantum dots are prepared in the organic solvent at high temperatures between 180 and 310°C, depending on the ligands and solvents employed in the preparation.

Quantum dots are nanoscale semiconductor crystals composed of Group II B (Transition metal)-Group VI A compounds (CdTe, CdS, CdHg, ZnS) or Group III A-Group V A elemental groups (InAs, InP, GaAs). A noble class of inorganic fluorophores is gaining widespread recognition as a result of their exceptional photophysical properties. Both the optical absorption and emission of quantum dots shift to the blue (higher energies) as the size of the dots gets smaller (Fig. 6) [147, 148].

Quantum dots have broad excitation spectrum; therefore, different-colored quantum dots can be activated by using a single source laser at the same time, making them extremely attractive in multiplexing studies [149–151]. For biological imaging applications, quantum dot materials are chosen based on size, optical properties, and toxicity. The emission wavelength should be in a region of the spectrum where blood and tissue absorb minimally but detectors are still efficient, approximately in the near-infrared (700–900 nm).

In spite of these attractive features the use of quantum dots in the biomedical application has been limited due to their hydrophobic character; now hydrophilic surface ligands, such as mercaptoacetic acid [152, 153] and polyethylene glycol (PEG), are used to increase their stability in aqueous media and to reduce the nonspecific adsorption. However, quantum dots capped with these small molecules are easily degraded by hydrolysis or oxidation of the capping ligands [153]. Heavy metal ions, such as Cd^{2+}, that can escape from the quantum dot matrix are cytotoxic and cause biocompatibility concerns [154, 155].

Molecular Probe/Polymer Composite Systems

Metal nanoparticles used in the biological imaging applications, such as gold and iron oxide, are easily cleared from the body because of biofouling of metal nanoparticles in the body.

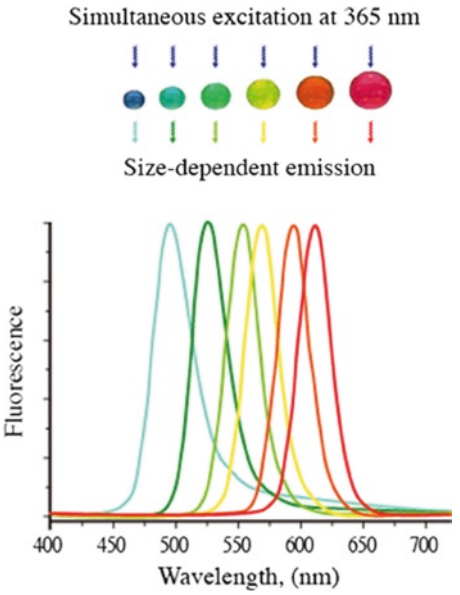

Fig. 6. Fluorescence spectra depending on the size of quantum dots [147, 148] (Blue fluorescence can be emitted from small particles of approximately 2 nm in diameter, green from ~3 nm particles, yellow from ~4 nm particles, and red from large particles of ~5 nm. The wavelength of the excitation light is 365 nm).

To overcome this limitation, the polymers used in the fabrication of hydrogels are utilized to stabilize the metal nanoparticles as molecular probe/polymer composite systems.

Contrast agents for Computer Tomography (CT) are based on iodinated small molecules because, among nonmetal atoms, iodine has a high X-ray absorption coefficient. However, iodinated compounds have very short imaging times due to rapid clearance by the kidney. Therefore, gold nanoparticles are used as they have a higher atomic number and X-ray absorption coefficient than iodine [156, 157]. However, gold nanoparticles also showed the rapid clearance by biofouling [158]. Gold nanoparticles can be combined with polymers containing thiol (-SH), which has a high affinity for gold atoms. Numerous modifications have been made based on this chemical nature of gold nanoparticles and this has led to several kinds of biosensors.

Poly(ethylene glycol)-SH (PEG-SH) can be design with CT contrast agents; the formation of PEG-coated gold nanoparticles enhances antibiofouling capability [159]. The X-ray absorption coefficient in vitro indicates that the attenuation of PEG-coated gold nanoparticles is 5.7 times higher than the iodine-based CT-contrast agent Ultravist in in-vivo animal test using rat.

The anionic character of gold nanoparticles stabilized with citrate attracts macromolecules with cationic character (positively charged polymers), such as chitosan and poly(ethyleneimine) (PEI). Through this electrostatic interaction gold nanoparticles/polymer composite systems are formed.

Multilayer film composites of gold nanoparticles and chitosan are constructed using layer by layer assembly [160]. The formation of the multilayer film was verified by UV–Vis Spectrometry, Atomic Force Microscopy, and Electrochemical Impedance Spectroscopy, and applied to nanodevices.

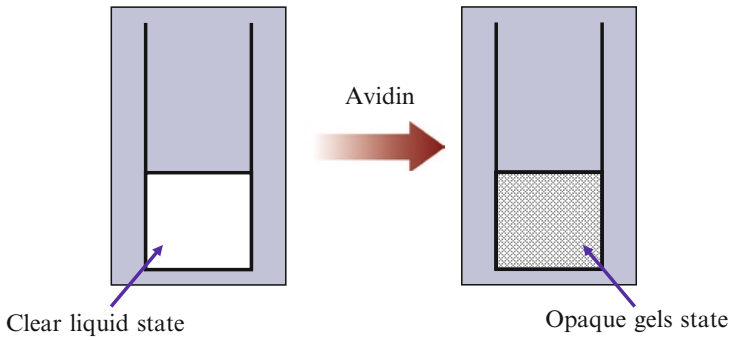

Fig. 7. Gold nanoparticles stabilized by biotinylated PNIPAM before and after the addition of avidin [161].

Gold nanoparticles protected/stabilized by biotinylated PNIPAM were prepared via a thiol anchoring end-group. The introduction of a biotin at the free chain-end of the stabilizer is to induce the supramolecular assembly containing gold nanoparticles via complexation with avidin in water [161].

As shown in Fig. 7, the gold nanoparticles stabilized by biotinylated PNIPAm demonstrated the nanostructure organization at the supramolecular level by biotin/avidin complexation in response to the biochemical species in the aqueous media, which can be utilized in the design of biosensors.

Iron Oxide Nanoparticle/Polymer Composite Systems

Iron oxide nanoparticles have been evaluated as an MRI contrast agent for the liver and the spleen. However, the applications are still subject to many limitations such as size monodispersity, magnetization, stability, nontoxicity, biocompatibility, injectability, and the short blood half-life of magnetic nanoparticles for in vivo applications. To overcome these limitations, a variety of biocompatible polymeric materials, such as PVP [162], Pluronic [163], dextran [164], chitosan [165], poly(D,L-lactid-co-glycolide) [166], and ε-caprolactone [167], have been employed as coating materials for MRI contrast agents.

Magnetic nanoparticles composites are prepared with Fe_3O_4 as core and chitosan as polymeric shell [168]. Chitosan and Fe_3O_4 aqueous suspensions are mixed in appropriate proportions using reverse-phase suspension crosslinking. The saturated magnetization of composite nanoparticles shows the characteristics of superparamagnets. The decrease in the saturated magnetization is related to the increased amounts of polymer incorporated in the polymer-coated magnetite suspension.

Similarly, sonochemistry can be employed to prepare iron oxide-loaded chitosan nanoparticles [165]. The magnetic Fe_3O_4 nanoparticles have been prepared by coprecipitation. Ferric chloride hexahydrate ($FeCl_3 \cdot 6H_2O$) and ferrous chloride tetrahydrate ($FeCl_2 \cdot 4H_2O$) are mixed with ammonium hydroxide (NH_4OH) under irradiated ultrasonic waves. The ferrofluid, made of iron oxide nanoparticles and chitosan, is sprayed on the surface of the alkali solution (NaOH/ethanol/water, 4/30/66, w/v/v) to form iron oxide-loaded chitosan nanoparticles.

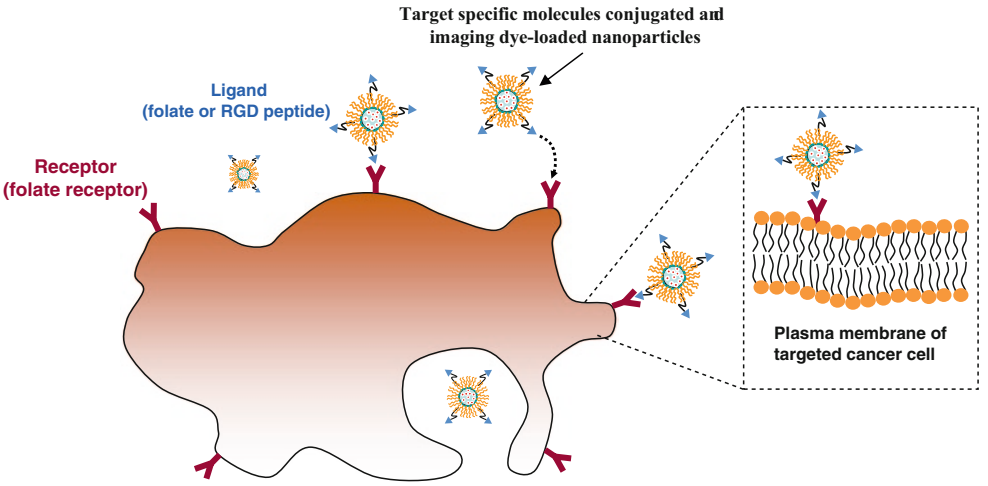

Fig. 8. Scheme of active cellular targeting [170].

These nanoparticles were injected into the left kidney of a rabbit and T2-weighted MR images of the kidney were obtained. The iron oxide-loaded chitosan nanoparticles enhanced contrast of the T2-weighted MR images.

Recently, active localizing imaging probes (gold nanoparticles and metal nanoparticles) in tumor tissue were accomplished by conjugating target specific molecules, such as folic acid [169], RGD peptide [170], or integrins [171] (Fig. 8).

The surface modification of iron oxide nanoparticles with folic acid was carried out to improve receptor binding and the efficiency of cellular internalization of nanoparticles [169]. To evaluate the targeting specificity of the nanoparticle–PEG–folic acid (NP–PEG–FA) conjugate to tumor cells, the uptake of the nanoconjugate by HeLa cells was compared with that by human osteosarcoma MG-63 cells (folate receptor negative cell line). Human osteosarcoma MG-63 cells express very low levels of the α and β forms of the folate receptor. The level of nanoparticle conjugate uptake by HeLa cells ranged from twice to as much as ten times that by MG-63 cells. Concomitant with this nanoparticle uptake, the T2-weighted MR phantom image showed a significant increase in the negative contrast enhancement of the HeLa cells compared with that of the MG-63 cells.

Quantum Dot/Polymer Composite Systems

Fluorescent semiconductor nanocrystals or quantum dots provide a new class of biomarkers that could overcome the limitations of organic dyes as in vitro and in vivo imaging probes. Despite of their advantages as a molecular probe, the semiconductor core of quantum dots has raised concerns regarding heavy metal cytotoxicity. In fact, quantum dots are cytotoxic due to cadmium oxidation and the leaching of heavy metal ions [171–173]. As quantum dots applications broaden in biotechnology research, it is important to consider these potential hazards and develop novel approaches to avoid toxicity, such as encapsulation or polymer coating, to form a protective insulating material or wide band gap semiconductor structurally matched with the core material.

The formation of quantum dot/polymer nanocomposites involves strong noncovalent interactions, such as hydrogen bonding, ionic attraction [174–176], and physically entrapping quantum dots into particles formed by emulsion polymerization [177] or sol–gel synthesis [178].

Quantum dot-encapsulated nanoparticles are noncytotoxic during long-term incubation with viable cells in the absence of light exposure, which makes them appropriate for cell monitoring and drug delivery [179, 180]. The quantum dots were conjugated with various molecules and proteins, such as myosin VI, transferin, and kinesin; when these bioconjugated quantum dots were present, receptor-mediated endocytosis occurred and the luminescent quantum dots enabled the investigation of cellular uptake pathways and detection within cells due to the bright fluorescence of the colloids. Since the quantum dots have broad excitation properties for all colors, multiple colors can be efficiently excited simultaneously with one light source, such as blue-violet filtered light or a 405 nm or 488 nm laser [181, 182].

Microbubble/Polymer Composite Systems

Ultrasound contrast agents are widely used to image perfusion and have potential for drug and gene delivery, where therapeutic release is initiated by local sonication [183–192]. Microbubble-loaded and lipid-based contrast agents have a self-assembled shell that provides a flexible, protective membrane around a perfluorocarbon gas core. In the diagnosis, these agents have been successfully used in the measurement of blood volume and flow in cardiology and radiology [192, 193].

Lipid-based microbubbles are usually stabilized with ligand and/or polymer molecules before bubble production, and the stabilized lipids are self-assembled into a shell with exposure to the aqueous medium. The approach for these lipid-stabilized contrast agents (diameters ~1–10) utilizes the lipid with PEG or PEG/ligand to specifically bind to a preferred target site [194].

Drug Delivery System with Molecular Imaging Capability

The development of noninvasive imaging technology (MRI, CT, PET, and Ultrasound) that integrates drug delivery systems with medical imaging is an important technology. A drug loaded with an imaging probe will enable real-time, targeted monitoring of drug delivery with medical imaging devices and to quantify drug uptake at the site as well as monitor the response to the therapy.

Yuk recently used composite gold nanoparticles, for the delivery of an anticancer drug; the ionic interaction between the gold nanoparticles and chitosan to form the composite nanoparticles loaded with paclitaxel [195]. Considering the optical property of gold nanoparticles, the gold nanoparticles/chitosan composite was utilized as a drug delivery system with molecular imaging capability (Fig. 9) [195].

The oleic acid (OA)-Pluronic (F-127)-coated iron oxide nanoparticles were formed with high doses of water insoluble doxorubicin [163]. Because of drug partitions into the OA shell, the surrounding iron oxide nanoparticles and the Pluronic anchor at the water–OA interface which significantly increased the solubility (dispersity) of the doxorubicin. Neither the formulation components nor the drug loading affected the magnetic properties of the core iron oxide nanoparticles and sustained release of doxorubin was observed 2 weeks under in vitro conditions. The nanoparticles in this study showed an enhanced intracellular drug retention, comparing with free drug in the aqueous solution, and a dose-dependent antiproliferative effect in breast and prostate cancer cell lines.

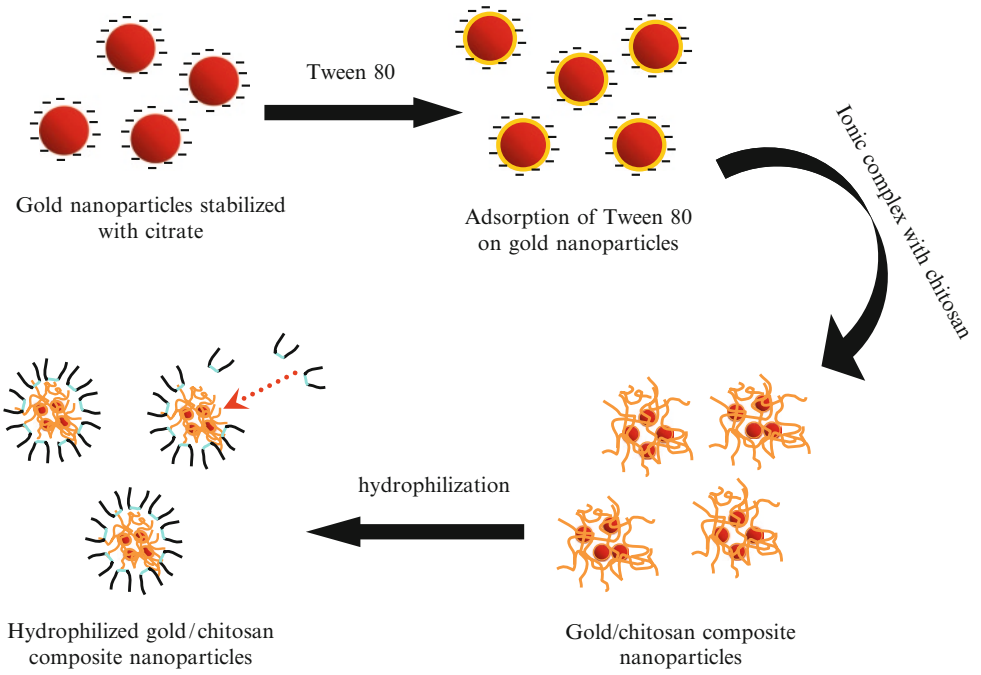

Fig. 9. Schematic description of gold/chitosan composite nanoparticles [195].

Doxorubicin-loaded superparamagnetic iron oxide (SPIO) nanoparticles were made using polymeric micelles with cRGD attached onto the surface of polymeric micelles for efficient targeting to tumors [196]. Amphiphilic block copolymers of maleimide-terminated poly(ethylene glycol)-block-poly(D,L-lactide) [MAL-PEG-PLA, Mn=7,200, Mn(PEG)=3,200] and methoxy-terminated poly-(ethylene glycol)-block-poly(D,L-lactide) copolymer [MPEG-PLA, Mn=6,400, Mn(PEG)=2,000] were used to form micelles with cRGD attached to the surface through a thiol-maleimide linkage. The cRGD on the surface of polymeric micelle targeted the delivery of doxorubicin to $\alpha_v\beta_3$-expressing tumor cells. The in vitro MRI and cytotoxicity of the $\alpha_v\beta_3$-specific cytotoxic response of these multifunctional polymeric micelles were observed by ultrasensitive MRI.

To combine contrast-enhanced ultrasound tumor imaging with targeted drug delivery is a challenging task [197–199]. Rapoport et al. developed novel ultrasound-sensitive multifunctional nanoparticles composed of nanoscale polymeric micelles that function as drug carriers and nano- or microscale echogenic bubbles that combine the properties of drug carriers, enhancers of ultrasound-mediated drug delivery with long-lasting ultrasound contrast agents [200, 201]. In their study, perfluoropentane (PFP) nanoemulsions dispersed in a solution of polymeric micelles were produced by introducing an aliquot of a sterilized PFP into a micellar solution of a copolymer which was subsequently subject to sonication to produce cavitation. Biodegradable diblock copolymers poly(ethylene oxide)-block-poly(lactide) and poly(ethylene oxide)-block-poly(caprolactone) were used to form polymeric micelles with doxorubicin as the drug model. The copolymer-stabilized PFP nanoemulsion systems undergo nanodroplet/nanobubble conversion in vivo, accumulate locally in the tumor tissue and coalesce into larger,

highly echogenic microbubbles, which provide long-lasting ultrasound contrast in the tumor while maintaining effective levels of doxorubicin at the tumor site.

The visualization and monitoring of transplanted islets using iron oxide nanoparticles covered with a modified dextran was carried out by incubating the Islets with magnetic nanoparticles consisting of a superparamagnetic iron core covered with a modified dextran coating [202]. The MRI showed a marked decrease in signal intensity on T2-weighted images at the implantation site in the left kidney as compared with the right kidney (implanted unlabeled islets). Thus, in vivo detection of transplanted human pancreatic islets using magnetic resonance imaging (MRI) that allowed noninvasive monitoring of islet grafts in diabetic mice in real time is now possible [202].

Summary

The unique feature of hydrogel-based drug delivery systems with molecular imaging capability involves loading a therapeutic agent into polymer network (hydrogels) surrounding molecular imaging probes. Although understanding and demonstrating the combination of hydrogels containing therapeutic agents with molecular imaging probes has been performed successfully, there remains the challenge for efficient application of this technology to diagnosis and therapy. The realization of hydrogels/molecular imaging probe composite systems on the nanoscale and the optimized drug release in response to the diagnosis is an important step. In the near future, this integrated smart system will open many potential opportunities for the effective therapeutic delivery and monitoring as well as molecular imaging probes for noninvasive procedures in early detection of disease.

References

1. Liu YY, Fan XD (2005) Synthesis, properties and controlled release behaviors of hydrogel networks using cyclodextrin as pendant groups. Biomaterials 26:6367–6374
2. John C, Lev EB, Edmond M (2003) Diffusion and release of solutes in pluronic-g-poly(acrylic acid) hydrogels. Langmuir 19:9162–9172
3. Alvarez-Lorenzoa C, Concheiroa A, Dubovik AS (2005) Temperature-sensitive chitosan-poly(*N*-isopropylacrylamide) interpenetrated networks with enhanced loading capacity and controlled release properties. J Control Release 102:629–641
4. Wang SC, Chen BH, Wang LF et al (2007) Release characteristics of lidocaine from local implant of polyanionic and polycationic hydrogels. J Control Release 118:333–339
5. Dayananda K, He C, Park DK et al (2008) pH- and temperature-sensitive multiblock copolymer hydrogels composed of poly(ethylene glycol) and poly(amino urethane). Polymer 49(23):4968–4973
6. Bhattarai N, Ramay HR, Gunn J et al (2005) PEG-grafted chitosan as an injectable thermosensitive hydrogel for sustained protein release. J Control Release 103:609–624
7. Zhang R, Tang M, Bowyer A et al (2005) A novel pH and ionic strength-sensitive carboxymethyl dextran hydrogel. Biomaterials 26:4677–4683
8. Mikos AG, Papadaki MG, Kouvrokoglou S (1994) Mini-review: islet transplantation to create a bioartificial pancreas. Biotechnol Bioeng 43:673–677
9. Laney MW, Kirsten NH, Kathryn H et al (2007) The effects of cell–matrix interactions on encapsulated b-cell function within hydrogels functionalized with matrix-derived adhesive peptides. Biomaterials 28:3004–3011
10. Hou QP, Bae YH (1999) Biohybrid artificial pancreas based on macrocapsule device. Adv Drug Deliv Rev 35:271–287

11. Chun MK, Cho CS, Choi HK (2002) Mucoadhesive drug carrier based on interpolymer complex of poly(vinyl pyrrolidone) and poly(acrylic acid) prepared by template polymerization. J Control Release 81:327–334
12. Siegel RA, Falamarzian M, Firestone BA et al (1988) pH controlled release from hydrophobic/polyelectrolyte copolymer hydrogel. J Control Release 8:179–182
13. Moneghini M, Voinovich D, Principalle F et al (2000) Formulation and evaluation of vinylpyrrolidone/vinylacetate copolymer microspheres with carbamazepine. Pharm Dev Technol 5:347–353
14. Torchilin VP, Shtilman MI, Trubetskoy VS et al (1994) Amphiphilic vinyl polymers effectively prolong liposome circulation time in vivo. Biochim Biophys Acta 1195:181–184
15. Kamada H, Tsutsumi Y, Yamamoto Y et al (2000) Antitumor activity of tumor necrosis factor-a conjugated with polyvinylpyrrolidone on solid tumors in mice. Cancer Res 60:6416–6420
16. D'souza AJM, Schowen RL, Topp EM (2003) Polyvinylpyrrolidone-drug conjugate: synthesis and release mechanism. J Control Release 94:91–100
17. Luo L, Ranger M, Lessard DG et al (2004) Novel amphiphilic diblock copolymer of low molecular weight poly(*N*-vinylpyrrolidone)-block-poly(D,L-lactide): synthesis, characterization, and micellization. Macromolecules 37:4008–4013
18. Lele BS, Leroux JC (2002) Synthesis and micellar characterization of novel amphiphilic A-B-A triblock copolymers of *N*-(2-Hydroxypropyl) methacrylamide or *N*-Vinyl-2-pyrrolidone with poly(ε-caprolactone). Macromolecules 35:6714–6723
19. Yokoyama F, Masada I, Shimamura K et al (1986) Morphology and structure of highly elastic poly-(vinyl alcohol) hydrogel prepared by repeated freezing-and-melting. Colloid Polym Sci 264:559–561
20. Hassan CM, Stewart JE, Peppas NA (2000) Diffusional characteristics of freeze/thawed poly(vinyl alcohol) hydrogels: applications to protein controlled release from multilaminate devices. Eur J Pharm Biopharm 49:161–165
21. Mansur HS, Sadahira CM, Souza AN et al (2008) FT-IR spectroscopy characterization of poly (vinyl alcohol) hydrogel with different hydrolysis degree and chemically crosslinked with glutaraldehyde. Mater Sci Eng C 28(4):539–548
22. Lin HL, Liu YF, Yu TL et al (2005) Light scattering and viscoelasticity study of poly(vinyl alcohol)-borax aqueous solutions and gels. Polymer 46:5541–5549
23. Mühlebach A, Müller B, Pharisa C et al (1997) New water-soluble photo crosslinkable polymers based on modified poly(vinyl alcohol). J Polym Sci A Polym Chem 35(16):3603–3611
24. Peppas NA, Wright SL (1996) Solute diffusion in poly(vinyl alcohol)/poly(acrylic acid) interpenetrating networks. Macromolecules 29:8798–8804
25. Peppas NA, Wright SL (1998) Drug diffusion and binding in ionisable interpenetrating networks from poly(vinyl alcohol) and poly(acrylic acid). Eur J Pharm Biopharm 4:15–29
26. Juntanon K, Niamlang S, Rujiravanit R et al (2008) Electrically controlled release of sulfosalicylic acid from crosslinked poly(vinyl alcohol) hydrogel. Int J Pharm 356:1–11
27. Yu FT, Yu MD, Xian WH et al (2007) Rheological characterisation of a novel thermosensitive chitosan/poly(vinyl alcohol) blend hydrogel. Carbohydr Polym 67:491–499
28. Wu G, Suc B, Zhang W et al (2008) In vitro behaviors of hydroxyapatite reinforced poly(vinyl alcohol) hydrogel composite. Mater Chem Phys 107:364–369
29. Kim JO, Park JK, Kim JH et al (2004) Development of poly(vinyl alcohol)-sodium alginate gel-matrix-based wound dressing system containing nitrofurazone. Polymer 45:7129–7136
30. Nishioa Y, Yamada A, Ezaki K et al (2004) Preparation and magnetometric characterization of iron oxide-containing alginate/poly(vinyl alcohol) networks. Polymer 45:7129–7136
31. Franssen O, van ooijen RD, de Boer D et al (1999) Enzymatic degradation of cross-linked dextrans. Macromolecules 32:2896–2902
32. Stenekes RJH, Loebis AE, Fernandes CM et al (2001) Degradable dextran microspheres for the controlled release of liposomes. Int J Pharm 214:17–20
33. van Dijk-Wolthuis WNE, Franssen O, Talsma H et al (1995) Synthesis, characterization and polymerization of glycidyl methacrylate derivatized dextran. Macromolecules 28:6317–6322
34. Massia SP, Stark J (2001) Immobilized RGD peptides on surface-grafted dextran promote biospecific cell attachment. J Biomed Mater Res 56(3):390–399
35. Rouzes C, Leonard M, Durand A et al (2003) Influence of polymeric surfactants on the properties of drug-loaded PLA nanospheres. Colloids Surf B 32:125–135
36. De Sousa DA, Leonard M, Dellacherie E (2001) Surface properties of polystyrene nanoparticles coated with dextrans and dextran-PEO Copolymers. Effect of polymer architecture on protein adsorption. Langmuir 17:4386–4391

37. De Sousa DA, Leonard M, Dellacherie E (2000) Surface modification of polystyrene nanoparticles using dextrans and dextran-POE copolymers: polymer adsorption and colloidal characterization. J Biomater Sci Polym Ed 11:1395–1410
38. Chen FM, Zhao YM, Sun HH et al (2007) Novel glycidyl methacrylated dextran (Dex-GMA)/gelatin hydrogel scaffolds containing microspheres loaded with bone morphogenetic proteins: Formulation and characteristics. J Control Release 118:65–77
39. Mitra S, Gaur U, Ghosh PC et al (2001) Tumour targeted delivery of encapsulated dextran–doxorubicin conjugate using chitosan nanoparticles as carrier. J Control Release 74:317–323
40. Barreiro-Iglesias R, Coronilla R, Concheiro A et al (2005) Preparation of chitosan beads by simultaneous cross-linking/insolubilisation in basic pH rheological optimisation and drug loading/release behaviour. Eur J Pharm Sci 24:77–84
41. Cho JH, Kim SH, Park KD et al (2004) Chondrogenic differentiation of human mesenchymal stem cells using a thermosensitive poly(*N*-isopropylacrylamide) and water-soluble chitosan copolymer. Biomaterials 25:5743–5751
42. Chung HJ, Go DH, Ba JW et al (2005) Synthesis and characterization of Pluronic grafted chitosan copolymer as a novel injectable biomaterial. Curr Appl Phys 5:485–488
43. Dufes C, Schätzlein AG, Tetley L et al (2000) Niosomes and polymeric chitosan based vesicles bearing transferring and glucose ligands for drug targeting. Pharm Res 17:1250–1258
44. Hejazi R, Amiji M (2003) Chitosan-based gastrointestinal delivery systems. J Control Release 89:151–165
45. Ormrod DJ, Holmes CC, Miller TE (1998) Dietary chitosan inhibits hypercholesterolaemia and atherogenesis in the apolipoprotein E-deficient mouse model of atherosclerosis. Atherosclerosis 138:329–334
46. Gallaher CM, Munion J, Hesslink R Jr et al (2000) Cholesterol reduction by glucomannan and chitosan is mediated by changes in cholesterol absorption and bile acid and fat excretion in rats. J Nutr 130:2753–2759
47. Chen AH, Liu SC, Chen CY et al (2008) Comparative adsorption of Cu(II), Zn(II), and Pb(II) ions in aqueous solution on the crosslinked chitosan with epichlorohydrin. J Hazard Mater 154(1–3):184–191
48. Chen F, Zhang ZR, Yuan F et al (2008) In vitro and in vivo study of *N*-trimethyl chitosan nanoparticles for oral protein delivery. Int J Pharm 349:226–233
49. Grant GT, Morris ER, Rees DA et al (1973) Biological interactions between polysaccharides and divalent cations: the egg-box model. FEBS Lett 32(1):195–198
50. Morris ER (1974) Molecular interactions in polysaccharide gelation. Br Polym J 18:14–21
51. Smidsrod O (1974) Molecular basis for some physical properties of alginates in gel state. Faraday Discuss Chem Soc 57:263–274
52. Ouwerx C, Velings N, Mestdagh MM et al (1998) Physico-chemical properties and rheology of alginate gel beads formed with various divalent cations. Polym Gels Netw 6:393–408
53. Montero P, Pérez-Mateos M (2002) Effects of Na^+, K^+ and Ca^{2+} on gels formed from fish mince containing a carrageenan or alginate. Food Hydrocol 16:375–385
54. Murata Y, Hirai D, Kofuji KE (2004) Properties of an alginate gel bead containing a chitosan-drug salt. Biol Pharm Bull 27:440–442
55. Murata Y, Jinno D, Kofuji K et al (2004) Properties of calcium-induced gel beads prepared with alginate and hydrolysates. Chem Pharm Bull 52:605–607
56. Liu X, Xu W, Liu Q et al (2004) Swelling behaviour of alginate–chitosan microcapsules prepared by external gelation or internal gelation technology. Carbohydr Polym 56:459–464
57. Lin YH, Liang HF, Chung CK et al (2005) Physical crosslinked alginate/*N*, *O*-carboxymethyl chitosan hydrogels with calcium for oral delivery of protein drugs. Biomaterials 26:2105–2113
58. Holte Ø, Onsøyen E, Myrvold R et al (2003) Sustained release of water-soluble drug from directly compressed alginate tablets. Eur J Pharm Sci 20:403–407
59. Bajpai SK, Shubhra S (2004) Investigation of swelling/degradation behaviour of alginate beads crosslinked with Ca^{2+} and Ba^{2+} ions. React Funct Polym 59:129–140
60. Denis D, van Mathieu S, Rose MG et al (2006) The influence of implantation site on the biocompatibility and survival of alginate encapsulated pig islets in rats. Biomaterials 27:3201–3208
61. Choi YH, Lee JH, Yuk SH (2006) Core/shell macrobeads for the protection of islets from immune system rejection. J Bioact Compat Polym 21:71–81
62. Koch S, Schwinger C, Kressler J et al (2003) Alginate encapsulation of genetically engineered mammalian cells: comparison of production devices, methods and microcapsule characteristics. J Microencapsul 20: 303–316
63. Xiong XY, Tam KC, Gan LH (2006) Polymeric nanostructures for drug delivery applications based on pluronic copolymer systems. J Nanosci Nanotechnol 6(9–10):2638–2650

64. Alexandridis P, Hatton TA (1995) Poly (ethylene oxide)–poly (propylene oxide)–poly (ethylene oxide) block copolymer surfactants in aqueous solutions and at interfaces: thermodynamics, structure, dynamics, and modeling. Colloids Surf A Physicochem Eng Asp 96:1–46
65. Ruel-Gariepy E, Leroux JC (2004) In situ-forming hydrogels-review of temperature-sensitive systems. Eur J Pharm Biopharm 58:409–426
66. Dumortier G, Grossiord JL, Agnely F et al (2006) A review of Poloxamer 407 pharmaceutical and pharmacological characteristics. Pharm Res 23:2709–2728
67. Newa M, Bhandari KH, Li DX (2007) Preparation, characterization and in vivo evaluation of ibuprofen binary solid dispersions with poloxamer 188. Int J Pharm 343(1–2):228–237
68. Yong CS, Oh YK, Kim YI et al (2005) Physicochemical characterization and in vivo evaluation of poloxamer-based solid suppository containing diclofenac sodium in rats. Int J Pharm 301(1–2):54–61
69. Kayes JB, Rawlins DA (1979) Adsorption characteristics of certain poloexyethylene polyoxypropylene block co-polymers on polysterene latex. Colloid Polym Sci 257:622–629
70. Li JT, Caldwell KD, Rapoport N (1994) Surface properties of pluronic-coated polymeric colloids. Langmuir 10:4475–4482
71. Illum L, Jacobsen LO, Muller RH et al (1987) Surface characteristics and the interaction of colloidal particles with mouse peritoneal macrophages. Biomaterials 8:113–117
72. Tan JS, Butterfield DE, Voycheck CL et al (1993) Surface modification of nanoparticles by PEO/PPO block copolymers to minimize interactions with blood components and prolong blood circulation in rats. Biomaterials 14:823–833
73. Stolnik S, Dunn SE, Garnett MC et al (1994) Surface modification of poly(lactide-co-glycolide) nanoparticles by biodegradable poly(lactide)-poly(ethylene glycol) copolymer. Pharm Res 11:1800–1808
74. Bazile D, Prud'homme C, Bassoullet MT et al (1995) Stealth Me.PEG-PLA nanoparticles avoid uptake by the mononuclear phagocyte system. J Pharm Sci 84:493–498
75. Jeong B, Bae YH, Kim SW (2000) Drug release from biodegradable injectable thermosensitive hydrogel of PEG–PLGA–PEG triblock copolymer. J Control Release 63:155–163
76. Jeong B, Bae YH, Kim SW (1999) Thermoreversible gelation of PEG–PLGA–PEG triblock copolymer aqueous solutions. Macromolecules 32:7064–7069
77. Lee DS, Shim MS, Kim SW et al (2001) Novel thermoreversible gelation of biodegradable PLGA-block–PEO-block–PLGA triblock copolymers in aqueous solution. Macromol Rapid Commun 22:587–592
78. Jeong B, Bae YH, Kim SW (2000) In situ gelation of PEG–PLGA–PEG triblock copolymer aqueous solutions and degradation thereof. J Biomed Mater Res 50:171–177
79. Kim SC, Kim DW, Shim YH et al (2001) In vivo evaluation of polymeric micellar paclitaxel formulation: toxicity and efficacy. J Control Release 72:191–202
80. Kim T, Kim D, Chung J (2004) Phase I and pharmacokinetic study of genexol-PM, a cremophor-free, polymeric micelleformulated paclitaxel, in patients with advanced malignancies. Clin Cancer Res 10:3708–3716
81. Heskins M, Guillet JJ (1968) Solution properties of poly(*N*-isopropylacrylamide). J Macromol Sci Part A Pure Appl Chem 2(8):1441–1455
82. Xu J, Ye J, Liu S (2007) Synthesis of well-defined cyclic poly(*N*-isopropylacrylamide) via click chemistry and its unique thermal phase transition behavior. Macromolecules 40(25):9103–9110
83. Feil H, Bae YH, Feijen J et al (1993) Effect of comonomer hydrophilicity and ionization on the lower critical solution temperature of *N*-isopropylacrylamide copolymers. Macromolecules 26(10):2496–2500
84. Zhang J, Pelton R, Deng Y (1995) Temperature-dependent contact angles of water on poly(*N*-isopropylacrylamide) gels. Langmuir 11(6):2301–2302
85. Maeda T, Kanda T, Yonekura Y et al (2006) Hydroxylated poly(*N*-isopropylacrylamide) as functional thermoresponsive materials. Biomacromolecules 7(2):545–549
86. Canavan HE, Cheng X, Graham DJ et al (2005) Surface characterization of the extracellular matrix remaining after cell detachment from a thermoresponsive polymer. Langmuir 21:1949–1955
87. Yoshida R, Uchida K, Kaneko Y et al (1995) Comb-type grafted hydrogels with rapid de-swelling response to temperature changes. Nature 374:240–242
88. Tuncel A, Ozdemir A (2000) Thermally reversible VPBA–NIPAM copolymer gels for nucleotide adsorption. J Biomater Sci Polym Ed 11:817–831
89. Lin HH, Cheng YL (2001) In-situ thermoreversible gelation of block and star copolymers of Poly(ethylene glycol) and Poly(*N*-isopropylacrylamide) of varying architectures. Macromolecules 34:3710–3715
90. Kwon OH, Kikuchi A, Yamato M et al (2000) Rapid cell sheet detachment from Poly(*N*-isopropylacrylamide)-grafted porous cell culture membranes. J Biomed Mater Res 50:82–89
91. Yamato M, Kwon OH, Hirose M et al (2000) Novel patterned cell coculture utilizing thermally responsive grafted polymer surfaces. J Biomed Mater Res 55:137–140

92. Shimizu T, Yamato M, Kikuchi A et al (2001) Two-dimensional manipulation of cardiac myocyte sheets utilizing temperature-responsive culture dishesauguments the pulsatile amplitude. Tissue Eng 7:141–151
93. Li C, Buurma NJ, Haq I et al (2005) Synthesis and characterization of biocompatible, thermoresponsive ABC and ABA triblock copolymer gelators. Langmuir 21(24):11026–11033
94. Hay DNT, Rickert PG, Seifert S et al (2004) Thermoresponsive nanostructures by self-assembly of a poly(*N*-isopropylacrylamide)-lipid conjugate. J Am Chem Soc 126(8):2290–2291
95. Jeong B, Choi YK, Bae YH et al (1999) New biodegradable polymers for injectable drug delivery systems. J Control Release 62:109–114
96. Lee SB, Park EK, Lim YM et al (2006) Preparation of alginate/poly(*N*-isopropylacrylamide) semi-interpenetrating and fully interpenetrating polymer network hydrogels with γ-ray irradiation and their swelling behaviors. J Appl Pol Sci 100:4439–4446
97. Kim MH, Kim JC, Lee HY et al (2005) Release property of temperature-sensitive alginate beads containing poly(*N*-isopropylacrylamide). Colloids Surf B Biointerfaces 46:57–61
98. Neradovic D, Soga O, van Nostrum CF et al (2004) The effect of the processing and formulation parameters on the size of nanoparticles based on block copolymers of poly(ethylene glycol) and poly(*N*-isopropylacrylamide) with and without hydrolytically sensitive groups. Biomaterials 25:2409–2418
99. Wei H, Zhang XZ, Zhou Y et al (2006) Selfassembled thermoresponsive micelles of poly(*N*-isopropylacrylamide-b-methyl methacrylate). Biomaterials 27:2028–2034
100. Kreibig U, Vollmer M (1996) Optical properties of metal clusters. Springer verlag, Berlin
101. Turkevich J, Stevenson PC, Hillier J (1951) A study of the nucleation and growth processes in the synthesis of colloidal gold. Discuss Faraday Soc 11:55
102. Shukla R, Bansal V, Chaudhary M et al (2005) Biocompatibility of gold nanoparticles and their endocytotic fate inside the cellular compartment: a microscopic overview. Langmuir 21:10644–10654
103. Connor EE, Mwamuka J, Gole A et al (2005) Gold nanoparticles are taken up by human cells but do not cause acute cytotoxicity. Small 1:325–327
104. Kim DK, Park SJ, Lee JH et al (2007) Antibiofouling polymer-coated gold nanoparticles as a contrast agent for in vivo X-ray computed tomography imaging. J Am Chem Soc 129:7661–7665
105. Raynal I, Prigent P, Peyramaure S et al (2004) Macrophage endocytosis of superparamagnetic iron oxide nanoparticles mechanisms and comparison of ferumoxides and ferumoxtran-10. Invest Radiol 39:56–63
106. Rogers WJ, Basu P (2005) Factors regulating macrophage endocytosis of nanoparticles: implications for targeted magnetic resonance plaque imaging. Atherosclerosis 178:67–73
107. Woodle MC, Engbers CM, Zalipsky S (1994) New amphipatic polymer-lipid conjugates forming long-circulating reticuloendothelial system-evading liposomes. Bioconjug Chem 5:493–496
108. Fong YC, Chia HS, Yu SY (2005) Characterization of aqueous dispersions of Fe_3O_4 nanoparticles and their biomedical applications. Biomaterials 26:729–738
109. Knag YS, Risbud S, Rabolt JF et al (1996) Synthesis and characterizations of nanometer-size Fe_3O_4 and Fe_2O_3 particles. Chem Mater 8:2209–2211
110. Mann S, Hannington JP (1988) Formation of iron oxides in unilamellar vesicles. J Colloid Interface Sci 122:326–335
111. Domingo C, Rodriguez Clemente R, Blesa MA (1993) Kinetics of oxidative precipitation of iron oxide particles. Colloids Surf A 79:177–189
112. Euliss LE, Grancharov SG, O'Brien S et al (2003) Cooperative assembly of magnetic nanoparticles and block copolypeptides in aqueous media. Nano Lett 3:1489–1493
113. Park J, An K, Hwang Y et al (2004) Ultra-large-scale syntheses of monodisperse nanocrystals. Nat Mater 3:891–895
114. Swadeshmukul S, Rovelyn T, Nikoleta T et al (2001) Synthesis and characterization of silica-coated iron oxide nanoparticles in microemulsion: the effect of nonionic surfactants. Langmuir 17:2900–2906
115. Li L, Choo ESG, Yi JB et al (2008) Superparamagnetic silica composite nanospheres (SSCNs) with ultrahigh loading of iron oxide nanoparticles via an oil-in-DEG microemulsion route. Chem Mater 20:6292–6294
116. Jolivet JP, Belleville P, Tronc E et al (1992) Influence of Fe(II) on the formation of the spinel iron oxide in alkaline medium. Clays Clay Miner 40:531–539
117. Cuyper MD, Joniau M (1988) Magnetoliposomes. Eur Biophys J 15:311–319
118. Massart R (1981) Preparation of aqueous magnetic liquids in alkaline and acidic media. IEEE Trans Magn 17:1247–1248
119. Shah PS, Holmes JD, Johnston KP et al (2002) Size-selective dispersion of dodecanethiol-coated nanocrystals in liquid and supercritical ethane by density tuning. J Phys Chem B 106:2545–2551
120. Kitchens C, McLeod MC, Roberts B (2003) Solvent effects on the growth and steric stabilization of copper metallic nanoparticles in AOT reverse micelle systems. J Phys Chem B 107:11331–11338

121. Summers M, Eastoe J, Davis S (2002) Formation of $BaSO_4$ nanoparticles in microemulsions with polymerized surfactant shells. Langmuir 18:5023–5026
122. Marchand KE, Tarret M, Lechaire JP et al (2003) Investigation of AOT-based microemulsions for the controlled synthesis of MoSx nanoparticles: an electron microscopy study. Colloids Surf A Physicochem Eng Asp 214:239–248
123. Husein M, Rodil E, Vera J (2003) Formation of silver chloride nanoparticles in microemulsions by direct precipitation with the surfactant counterion. Langmuir 19:8467–8474
124. Charinpanitkul T, Chanagul A, Dutta J et al (2005) Effects of cosurfactant on ZnS nanoparticle synthesis in microemulsion. Sci Technol Adv Mater 6:266–271
125. Pileni MP (2003) The role of soft colloidal templates in controlling the size and shape of inorganic nanocrystals. Nat Mater 2:145–150
126. Singh R, Kumar S (2006) Effect of mixing on nanoparticle formation in micellar route. Chem Eng Sci 61:192–204
127. Wang YX, Hussain SM, Krestin GP (2001) Superparamagnetic iron oxide contrast agents: physicochemical characteristics and applications in MR imaging. Eur Radiol 11:2319–2331
128. Stark DD, Weissleder R, Elizondo G et al (1988) Superparamagnetic iron oxide: clinical application as a contrast agent for MR imaging of the liver. Radiology 168:297–301
129. Hamm B, Staks T, Taupitz M et al (1994) Contrast-enhanced MR imaging of liver and spleen: first experience in humans with a new superparamagnetic iron oxide. J Magn Reson Imag 4:659–668
130. Weissleder R, Bogdanov A, Neuwelt EA (1995) Long-circulating iron oxides for MR imaging. Adv Drug Deliv Rev 16:321–334
131. Wilson SR, Burnes PN, Muradali D et al (2000) Harmonic hepatic US with microbubble contrast agent: initial experience showing improved characterization of hemangioma, hepatocellular carcinoma, and metastasis. Radiology 215:153–161
132. Kedar RP, Cosgrove D, McCready VR et al (1996) Microbubble contrast agent for color Doppler US: effect on breast masses. Work in progress. Radiology 198:679–686
133. Halpern EJ, Rosenberg M, Gomella LG (2001) Prostate cancer: contrast-enhanced US for detection. Radiology 219:219–225
134. Ellegala DB, Leong-Poi H, Carpenter JE et al (2003) Imaging tumor angiogenesis with contrast ultrasound and microbubbles targeted to alpha(v)beta3. Circulation 108:336–341
135. Leong-Poi H, Christiansen J, Klibanov AL et al (2003) Noninvasive assessment of angiogenesis by ultrasound and microbubbles targeted to alpha(v)-integrins. Circulation 107:455–460
136. Weller GER, Wong MKK, Modzelewski RA et al (2005) Ultrasonic imaging of tumor angiogenesis using contrast microbubbles targeted via the tumor-binding peptide arginine–arginine–leucine. Cancer Res 65:533–539
137. Stieger SM, Dayton PA, Borden MA et al (2007) Imaging of angiogenesis using cadence contrast pulse sequencing and targeted contrast agents. Contrast Media Mol Imaging 3(1):9–18
138. Unger E, Metzger P, Krupinski E et al (2000) The use of a thrombus-specific ultrasound contrast agent to detect thrombus in arteriovenous fistulae. Invest Radiol 35:86–89
139. Lindner JR, Song J, Christiansen J et al (2001) Ultrasound assessment of inflammation and renal tissue injury with microbubbles targeted to P-selectin. Circulation 104:2107–2112
140. Linker RA, Reinhardt M, Bendszus M et al (2005) In vivo molecular imaging of adhesion molecules in experimental autoimmune encephalomyelitis (EAE). J Autoimmun 25:199–205
141. Takalkar AM, Klibanov AL, Rychak JJ et al (2004) Binding and detachment dynamics of microbubbles targeted to P-selectin under controlled shear flow. J Control Release 96:473–482
142. Rychak JJ, Li B, Acton ST et al (2006) Selectin ligands promote ultrasound contrast agent adhesion under shear flow. Mol Pharmacol 3:516–524
143. Lankford M, Behm CZ, Yeh J et al (2006) Effect of microbubble ligation to cells on ultrasound signal enhancement: implications for targeted imaging. Invest Radiol 41(10):721–728
144. Rychak JJ, Lindner JR, Ley K et al (2006) Deformable gas-filled microbubbles targeted to P-selectin. J Control Release 114(3):288–299
145. Klibanov AL (2005) Ligand-carrying gas-filled microbubbles: ultrasound contrast agents for targeted molecular imaging. Bioconjug Chem 16:9–17
146. Rychak JJ, Klibanov AL, Ley KF et al (2007) Enhanced targeting of ultrasound contrast agents using acoustic radiation force. Ultrasound Med Biol 33(7):1132–1139
147. Bakalova R, Zhelev Z, Ohba H et al (2005) Quantum dot-based western blot technology for ultrasensitive detection of tracer proteins. J Am Chem Soc 127(26):9328–9329
148. Zhelev Z, Bakalova R, Ohba H (2006) Uncoated, broad fluorescent, and size-homogeneous CdSe quantum dots for bioanalyses. Anal Chem 78(1):321–330

149. Mingyong H, Xiaohu G, Jack ZS (2001) Quantum-dot-tagged microbeads for multiplexed optical coding of biomolecules. Nat Biotechnol 19:631–635
150. Bruchez M Jr, Moronne M, Gin P (1998) Semiconductor nanocrystals as fluorescent biological labels. Science 281:2013–2016
151. Han M, Gao X, Su JZ (2001) Quantum-dot-tagged microbeads for multiplexed optical coding of biomolecules. Nat Biotechnol 19:631–635
152. Chan WC, Nie S (1998) Quantum dot bioconjugates for ultrasensitive nonisotopic detection. Science 281:2016–2018
153. Chen Y, Rosenzweig Z (2002) Luminescent CdSe quantum dot doped stabilized micelles. Nano lett 2(11):1299–1302
154. Kirchner C, Liedl T, Kudera S et al (2005) Cytotoxicity of colloidal CdSe and CdSe/ZnS nanoparticles. Nano Lett 5:331–338
155. O'Brien P, Cummins SS, Darcy D et al (2003) Quantum dot-labelled polymer beads by suspension polymerization. Chem Commun 3:2532–2533
156. Rabin O, Manuel Perez J, Grimm J (2006) An X-ray computed tomography imaging agent based on long-circulating bismuth sulphide nanoparticles. Nat Mater 5(2):118–122
157. Hainfeld JF, Slatkin DN, Focella TM (2006) Gold nanoparticles: a new X-ray contrast agent. Br J Radiol 79(939):248–253
158. Lee HR, Lee EH, Kim DK et al (2006) Antibiofouling polymer-coated superparamagnetic iron oxide nanoparticles as potential magnetic resonance contrast agents for in vivo cancer imaging. J Am Chem Soc 128:7383–7389
159. Kim DK, Park SJ, Lee JH et al (2007) Antibiofouling polymer-coated gold nanoparticles as a contrast agent for in vivo X-ray computed tomography imaging. J Am Chem Soc 29:7661–7665
160. Huang H, Yang X (2003) Chitosan mediated assembly of gold nanoparticles multilayer. Colloids Surf A Physicochem Eng Asp 226(1–3):77–86
161. Aqil A, Qiu H, Greisch JF et al (2008) Coating of gold nanoparticles by thermosensitive poly(*N*-isopropylacrylamide) end-capped by biotin. Polymer 49:1145–1153
162. Lee HY, Lee SH, Xu C et al (2008) Synthesis and characterization of PVP-coated large core iron oxide nanoparticles as an MRI contrast agent. Nanotechnology 19:165101–165107
163. Jain TK, Morales MA, Sahoo SK et al (2005) Iron oxide nanoparticles for sustained delivery of anticancer agents. Mol Pharm 2(3):194–205
164. Dutza S, Andrä W, Hergta R et al (2007) Influence of dextran coating on the magnetic behaviour of iron oxide nanoparticles. J Magn Magn Mater 311:51–54
165. Kim EH, Ahn YK, Lee HS (2007) Biomedical applications of superparamagnetic iron oxide nanoparticles encapsulated within chitosan. J Alloys Compd 434–435:633–636
166. Patel D, Moon JY, Chang YM et al (2008) Poly(D,L-lactide-co-glycolide) coated superparamagnetic iron oxide nanoparticles: synthesis, characterization and in vivo study as MRI contrast agent. Colloids Surf A Physicochem Eng Asp 313–314:91–94
167. Yang X, Chen Y, Yuan R et al (2008) Folate-encoded and Fe_3O_4-loaded polymeric micelles for dual targeting of cancer cells. Polymer 49:3477–3485
168. Li GY, Jiang YR, Huang KL et al (2008) Preparation and properties of magnetic Fe_3O_4-chitosan nanoparticles. J Alloys Compd 466(1–2):451–456
169. Conroy S, Raymond S, Miqin Z (2006) Folic acid-PEG conjugated superparamagnetic nanoparticles for targeted cellular uptake and detection by MRI. J Biomed Mater Res 78A:550–570
170. Peer D, Karp JM, Hong SP et al (2007) Nanocarriers as an emerging platform for cancer therapy. Nat Nanotechnol 2:751–760
171. Norased N, Erik B, Jimin R (2006) Multifunctional polymeric micelles as cancer-targeted, MRI-ultrasensitive drug delivery systems. Nano Lett 6(11):2427–2430
172. von zur Muhlena C, von Elverfeldt D, Bassler N et al (2007) Superparamagnetic iron oxide binding and uptake as imaged by magnetic resonance is mediated by the integrin receptor Mac-1 (CD11b/CD18): implications on imaging of atherosclerotic plaques. Atherosclerosis 193:102–111
173. Derfus AM, Chan WCW, Bhatia SN (2004) Probing the cytotoxicity of semiconductor quantum dots. Nano Lett 4:11–18
174. Hardman RA (2006) Toxicological review of quantum dots: toxicity depends on physicochemical and environmental factors. Environ Health Perspect 114:165–172
175. Guo G, Liu W, Liang J et al (2006) Preparation and characterization of novel CdSe quantum dots modified with poly(D,L-lactide) nanoparticles. Mater Lett 60:2565–2568
176. Zhang H, Wang C, Li M et al (2005) Fluorescent nanocrystal–polymer composites from aqueous nanocrystals: methods without ligand exchange. Chem Mater 17:4783–4788

177. Zhang H, Wang C, Li M et al (2005) Fluorescent nanocrystal–polymer complexes with flexible processability. Adv Mater 17:853–857
178. Gong Y, Gao M, Wang D et al (2005) Incorporating fluorescent CdTe nanocrystals into a hydrogel via hydrogen bonding: toward fluorescent microspheres with temperature-responsive properties. Chem Mater 17:2648–2653
179. Yang X, Zhang Y (2004) Encapsulation of quantum nanodots in polystyrene and silica micro-/nanoparticles. Langmuir 20:6071–6073
180. Mokari T, Sertchook H, Aharoni A et al (2005) Nano@micro: general method for entrapment of nanocrystals in sol–gel-derived composite hydrophobic silica spheres. Chem Mater 17:258–263
181. Watanabe TM, Higuchi H (2007) Stepwise movements in vesicle transport of HER2 by motor proteins in living cells. Biophys J 92:4109–4120
182. Bruchez MP (2005) Turning all the lights on: quantum dots in cellular assays. Curr Opin Chem Biol 9(5):533–537
183. Tartis MS, McCallan J, Lum AF et al (2006) Therapeutic effects of paclitaxel-containing ultrasound contrast agents. Ultrasound Med Biol 32(11):1771–1780
184. Chen SY, Ding JH, Bekeredjian R et al (2006) Efficient gene delivery to pancreatic islets with ultrasonic microbubble destruction technology. Proc Natl Acad Sci U S A 103(22):8469–8474
185. Kimmel E (2006) Cavitation bioeffects. Crit Rev Biomed Eng 34(2):105–161
186. Kipshidze NN, Porter TR, Dangas G et al (2005) Novel site-specific systemic delivery of Rapamycin with perfluorobutane gas microbubble carrier reduced neointimal formation in a porcine coronary restenosis model. Catheter Cardiovasc Interv 64(3):389–394
187. Korpanty G, Chen S, Shohet RV et al (2005) Targeting of VEGF-mediated angiogenesis to rat myocardium using ultrasonic destruction of microbubbles. Gene Ther 12(17):1305–1312
188. Unger EC, Hersh E, Vannan M et al (2001) Local drug and gene delivery through microbubbles. Prog Cardiovasc Dis 44(1):45–54
189. Kheirolomoom A, Dayton PA, Lum AFH et al (2007) Acoustically-active microbubbles conjugated to liposomes: characterization of a proposed drug delivery vehicle. J Control Release 118(3):275–284
190. Lee LY, Wang CH, Smith KA (2008) Supercritical antisolvent production of biodegradable micro- and nanoparticles for controlled delivery of paclitaxel. J Control Release 125:96–106
191. Suzaki R, Takizawa T, Negishi Y et al (2008) Tumor specific ultrasound enhanced gene transfer in vivo with novel liposomal bubbles. J Control Release 125:137–144
192. Leong-Poi H, Song J, Rim SJ et al (2002) Influence of microbubble shell properties on ultrasound signal: implications for low-power perfusion imaging. J Am Soc Echocardiogr 15(10):1269–1276
193. Brannigan M, Burns PN, Wilson SR (2004) Blood flow patterns in focal liver lesions at microbubble-enhanced US. Radiographics 24(4):921–935
194. Toublan FJJ, Boppart SA, Suslick KS (2006) Tumor targeting by surface-modified protein microspheres. J Am Chem Soc 128:3472–3473
195. Oh KS, Kim RS, Yuk SH et al (2008) Gold/chitosan/pluronic composite nanoparticles for drug delivery. J Appl Polym Sci 108:3239–3244
196. Nasongkla N, Bey E, Ren J et al (2006) Multifunctional polymeric micelles as cancer-targeted, MRI-ultrasensitive drug delivery systems. Nano Lett 6(11):2427–2430
197. Ungar EC, Porter T, Culp W et al (2004) Therapeutic applications of lipid-coated microbubbles. Adv Drug Deliv Rev 56:1291–1314
198. Lum AFH, Borden MA, Dayton PA et al (2006) Ultrasound radiation force enables targeted deposition of model drug carriers loaded on microbubbles. J Control Release 111:128–134
199. Shortencarier MJ, Dayton PA, Bloch SH et al (2004) A method for radiation-force localized drug delivery using gas-filled lipospheres. IEEE Trans Ultrason Ferroelectr Freq Control 51(7):822–831
200. Rapoport N, Gao Z, Kennedy A (2007) Multifunctional nanoparticles for combining ultrasonic tumor imaging and targeted chemotherapy. J Natl Cancer Inst 99(14):1095–1106
201. Gao Z, Fain H, Rapoport N (2005) Controlled and targeted tumor chemotherapy by micellar-encapsulated drug and ultrasound. J Control Release 102:203–221
202. Brad PB, Aravind A, Parag V et al (2007) Magnetic resonance-guided, real-time targeted delivery and imaging of magnetocapsules immunoprotecting pancreatic islet cells. Nat Med. doi:10.1038/nm1581